Materials Science & Engineering C 104 (2019) 110000

Contents lists available at ScienceDirect

Materials Science & Engineering C

journal homepage: www.elsevier.com/locate/msec

MXene-Ti_3C_2/CuS nanocomposites: Enhanced peroxidase-like activity and sensitive colorimetric cholesterol detection

Yapeng Li[a,1], Zewen Kang[b,1], Lingyao Kong[a], Huiting Shi[a], Yanzhou Zhang[a,*], Malin Cui[b], Da-Peng Yang[b,*]

[a] Department of Cardiology, The First Affiliated Hospital of Zhengzhou University, Zhengzhou, China
[b] College of Chemical Engineering and Materials Science, Quanzhou Normal University, Quanzhou, Fujian Province, China

ARTICLE INFO

Keywords:
MXene
Ti_3C_2
CuS
Colorimetric detection
Cholesterol

ABSTRACT

Nanomaterials with enzyme-like activity have attracted much attention recently. Herein, we report the synthesis of a new type of 2D MXene-Ti_3C_2/CuS nanocomposites with peroxidase-like activity using a simple hydrothermal approach. Significantly, compared with the individual MXene-Ti_3C_2 nanosheets or CuS nanoparticles, the MXene-Ti_3C_2/CuS nanocomposites show a synergistically enhanced peroxidase-like activity and can be used as an efficient mimetic peroxidase to catalyze the reaction of 3,3,5,5-tetramethylbenzidine (TMB) in the presence of hydrogen peroxide (H_2O_2), causing a blue color change. Kinetic studies reveal that the MXene-Ti_3C_2/CuS nanocomposites have a higher catalytic activity to TMB than their single components, and the catalytic reaction follows the ping-pong mechanism. The MXene-Ti_3C_2/CuS nanocomposites are used for the colorimetric determination of cholesterol with a linear range of 10–100 μM and a limit of detection (LOD) of 1.9 μM. Our results show that the MXene-Ti_3C_2/CuS nanocomposites based colorimetric cholesterol biosensor is cost-effective, sensitive, and selective, which has potential application in H_2O_2 and cholesterol detection and clinic medicine diagnostics.

1. Introduction

Cholesterol (belonging to a sterol in scientific terms) is one of important components in cell membranes, which is transported in the blood plasma of mammals. An abnormal level of cholesterol is possibly closely associated with some diseases, such as atherosclerosis, hypertension, stroke etc. Therefore, to accurately monitor the level of cholesterol in blood plasma has aroused more and more attention in medical diagnostics and therapy [1–4]. Currently, some various methods/techniques have been developed for cholesterol detection, such as electrochemical, fluorescence, liquid-phase chromatographic, as well as colorimetric methods [5–9]. Among these methods, colorimetric detection is of great interest for cholesterol determination owing to its advantages of simplicity, low-cost, as well as high sensitivity and selectivity [10–12]. Colorimetric assays are carried out utilizing some particular visualization reagents that experience a color change in the presence of an analyte. The color change can be accurately and easily measured by UV–vis spectrum. Therefore, the advantage of this method is rather obvious for hydrogen peroxide detection, which is one of important small molecular compounds in the fields of food, textile, pharmaceutical, environmental as well as medicine [13–17]. It is also a product generated during the oxidation of substrates catalyzed by enzymes such as cholesterol oxidase, glucose oxidase, xanthine oxidase, etc. Therefore, to accurately determine the level of hydrogen peroxide can indirectly measure the level of target molecules (such as glucose, cholesterol, xanthine, etc.) in some related studies. The chromogenic reagent 3,3,5,5-tetramethylbenzidine (TMB) is often used as a substrate for H_2O_2 detection in the presence of peroxidase. Peroxidase is a kind of enzyme, which can catalyze the reaction of peroxidase substrate-TMB in the presence of H_2O_2 to produce a blue color reaction. However, some inherent disadvantages such as low-stability, high-costs as well as difficult preparation largely hindered its wide application. Therefore, looking for efficient enzyme mimetics is becoming an increasingly important goal in bioassays and medicine diagnostics [18–24]. With the rapid development of nanotechnology, some nanomaterials with enzyme-like properties have attracted much attention [23,25–28]. For example, metal nanoparticles (Au, Pt, etc.) [29,30], carbon-based nanomaterials (graphene oxide, graphene quantum dots) [31–33], metal oxides (CeO_2, Fe_3O_4)/sulfides [19,34], nanoparticles (CuS, CoS) [35,36], etc. were widely reported to mimetic the function of enzymes.

* Corresponding authors.
E-mail addresses: zhangyzxnk@163.com (Y. Zhang), yangdp@qztc.edu.cn (D.-P. Yang).
[1] Zewen Kang and Yapeng Li contributed equally to this work.

https://doi.org/10.1016/j.msec.2019.110000
Received 4 January 2019; Received in revised form 3 July 2019; Accepted 18 July 2019
Available online 19 July 2019

Among these nanomaterials-based enzyme mimetics, a new generation of nanocomposites is of particular interest due to their high catalysis activities. It is believed that nanocomposites can bring about synergistic effect of each component or give rise to an enhanced performance. Up to now, many different types of nanocomposites with enhanced enzyme-like properties have been applied for colorimetric detection assays. Typically, Dong et al. prepared highly dispersed CeO_2–nanotube TiO_2 nanocomposites with peroxidase-like property for colorimetric detection of H_2O_2 and glucose [34]. Lu et al. fabricated cobalt ferrite/cobalt sulfide hybrid nanotubes with enhanced peroxidase-like activity for colorimetric detection of dopamine. Owing to the synergistic effect between each component, the prepared nanocomposites exhibited enhanced peroxidase-like activity, exceeding that of either the individual component alone [37]. Saxena et al. reported a nanocomposite with Gold nanoparticles supported on MoS_2 nanoribbons with enhanced colorimetric sensing of free cholesterol in human serum [5]. Obviously, the effective combination and strong interaction between nanoparticles and 2D nanomaterials is a promising strategy for designing or fabricating enzyme mimetics with superior performance [38,39]. MXene is a new 2D transition metal carbide or nitride nanomaterial showing intriguing metallic conductivity, stability, large surface area and ease of functionalization, hydrophilicity as well as biocompatibility [40]. With a layered structure similar to that of graphene, it has been widely explored in the field of energy, nanomedicine, catalysis and sensing. Particularly, MXene is regarded as fascinating interface for sensing application with the advantages of rapid, easy, and label-free detection [41–43]. However, for the colorimetric sensing, the original MXene did not enable TMB to produce a blue color reaction in the presence of H_2O_2. Therefore, in order to extend its application potential, further surface modifications or fabricating MXene-based nanocomposites might become a best choice for colorimetric biosensor.

CuS is an important p-type semiconductor, possessing distinct electronic and optical properties. Due to its low toxicity and production cost, simple preparation, as well as strong near-infrared absorbance, CuS nanoparticles have essential application value in the field of nanomedicine [44]. Intriguingly, CuS nanoparticles have been proved to have peroxidase-like activity. And, the diversely sized CuS nanomaterials exhibited different peroxidase-like activity. [45]. Given this, the efficient combination of MXene and CuS nanoparticles might further improve their peroxidase-like property and be in favor of developing highly sensitive glucose or cholesterol sensors with good compatibility. To the best of our knowledge, there are no reports on the synthesis and use of MXene-Ti_3C_2/CuS nanocomposites for colorimetric applications. Herein, we report, for the first time, on the exploring of MXene-Ti_3C_2/CuS nanocomposites for sensitive colorimetric H_2O_2 and cholesterol detection. The nanocomposites are synthesized via a hydrothermal method. The morphology and structure are characterized by SEM, XRD and XPS. Colorimetric assay indicates that the as-prepared MXene-Ti_3C_2/CuS nanocomposites have an enhanced peroxidase activity compared with their individual component. Also, the effects of pH, temperature and salt concentrations are evaluated for peroxidase activity, and a catalysis reaction mechanism is discussed. Last, colorimetric cholesterol detection in human serum is determined using the nanocomposites (Scheme 1).

2. Experimental section

2.1. Materials and agents

Ti_3AlC_2 (powder, 200-meshes) was purchased from Forsman Scientific (Beijing, China). Hydrochloric acid (HCl) (purity > 98%) was purchased from Lingfeng Chemical Reagent Co., Ltd. (Shanghai, China). LiF, $AlCl_3{\cdot}6H_2O$ and TMAOH (tetramethylammonium hydroxide ($C_4H_{13}NO$)) were purchased from Admas (America). 3,3′,5,5′-Tetramethylbenzidine (TMB), *o*-phenylenediamine (OPD) and 2,2′-azino-bis(3-ethylbenzothiazoline-6-sulfonic acid) (ABTS) were purchased from Aladdin (Shanghai, China). Hydrogen peroxide (H_2O_2), acetic acid (HAc), sodium acetate (NaAc), sodium chloride (NaCl), ethylene glycol (EG), ethanol, absolute ethanol (C_2H_5OH), acetone (CH_3COCH_3), sulfur powder, cholesterol, ascorbic acid, uric acid, glucose, cysteine, serine and copper nitrate in trihydrate ($Cu(NO_3)_2{\cdot}3H_2O$) were purchased from Sinopharm Chemical Reagent Co., Ltd. (Shanghai, China). Cholesteroloxidase (CHOx, 100 UN) and cholesterol esterase (1 KU) were purchased from Sigma Aldrich. All chemicals were used as received without further treatment unless otherwise stated.

2.2. Instrumentation

A series of characterizations of as-prepared nanomaterials were performed via field-emission scanning electron microscopy (FE-SEM, Zeiss, Germany) with Energy Dispersive X-Ray Spectroscopy (EDS, OXFORD 51-XMX), X-ray powder diffraction (XRD, D8 ADVANCE, Bruker), UV–vis spectra (UV-2600, Shimadzu), X-ray photoelectron spectroscopy (XPS, (Physical Electronics, USA), Fourier transform infrared spectroscopy (FT-IR, a Nicolet AVATAR 360 FT-IR spectrometer) and Laser confocal Raman spectrometer (Renishaw, inVia).

2.3. Synthesis of MXene-Ti_3C_2

The MXene-Ti_3C_2 nanocomposites were prepared according to Dong's method [46]. Typically, 1.0 g of Ti_3AlC_2, LiF and $AlCl_3{\cdot}6H_2O$ powders were mixed with a mass ratio of 1:1:0.3, the mixture solution was etched in 10 mL of 9 M HCl for three days at room temperature. After collecting them by strong centrifugation, the obtained materials were washed with deionized water and anhydrous ethanol at least three times, respectively and then dispersed in 10 mL of TMAOH with a 25 wt % in deionized water for three days with continuous stirring. The intercalated MXene-Ti_3C_2 nanocomposites were collected by centrifugation and washed as above mentioned. Finally, the obtained accordion-like solid was decentralized into deionized water under ultrasonic for several hours, and then was centrifugated at 7000 rpm, a resulting colloidal dispersion of MXene-Ti_3C_2 nanosheets was collected.

2.4. Synthesis of MXene-Ti_3C_2/CuS nanocomposites and CuS nanoparticles

The MXene-Ti_3C_2/CuS nanocomposites were synthesized by a hydrothermal process. The as-prepared MXene-Ti_3C_2 was mixed with $Cu(NO_3)_2{\cdot}3H_2O$ and sulfur powders in a 1:10:1 mass ratios, which were subsequently dissolved in 35 mL ethylene glycol (EG), and under vigorous stirring for 30 min. Afterward, the solution was transferred into a 50 mL Teflon-lined stainless-steel autoclave quickly and maintained at 160 °C for 24 h, the black solid products were collected by centrifuging at 5000 rpm for several times. Finally, these MXene-Ti_3C_2/CuS solid products were then washed with distilled water, absolute ethanol and acetone three times each and dried in a vacuum oven at 80 °C for 6 h before other further characterizations. The synthesis of CuS is similar to the aforementioned method, the only difference is that no MXene-Ti_3C_2 nanosheets were added in the preparation process.

2.5. Colorimetric analysis

In order to confirm the colorimetric reaction of MXene-Ti_3C_2/CuS nanocomposites, the UV–vis absorbance of the oxidized TMB were tested at 652 nm in the absence or presence of H_2O_2 (200 μL). The time-dependent UV–vis spectra and absorbance changes were carried out at 30 °C by adding 10 μL MXene-Ti_3C_2/CuS nanocomposites in a reaction with 2 mL HAc-NaAc buffer (0.2 M, pH 3.5) and 200 μL TMB (1.2 mM) as substrates. The time-dependent UV–vis spectra were set for the parameters to automatically scan every 2 min. The typical Michaelies-Menten curves and double reciprocal plots of activity of MXene-Ti_3C_2/CuS with the concentration of H_2O_2 or TMB fixed were also measured. We also investigated the effects of pH (3.0–5.0), temperature

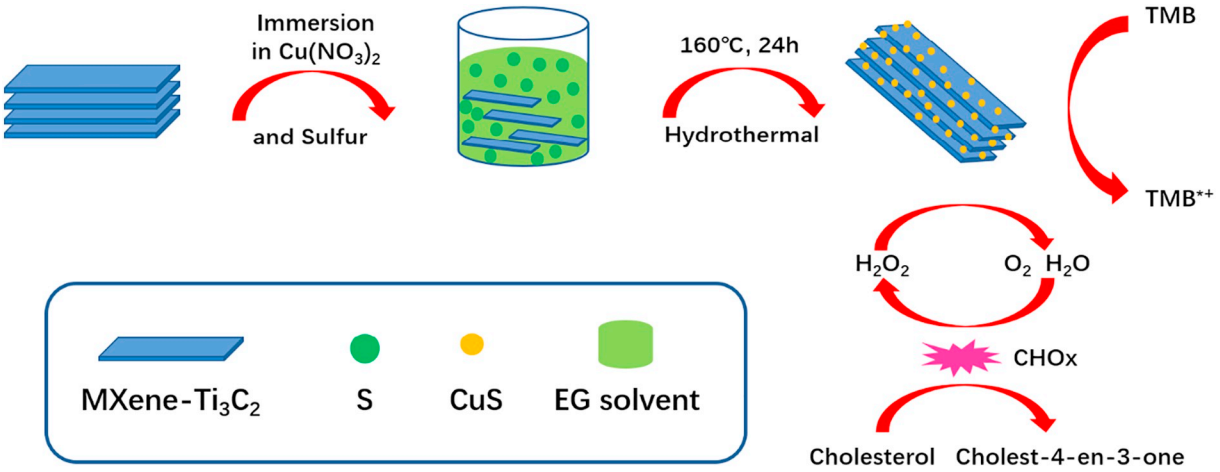

Scheme 1. Schematic illustration of preparation process of MXene-Ti_3C_2/CuS nanocomposites and its use for colorimetric cholesterol detection.

(30 °C–55 °C) and H_2O_2 concentration (0.1–1 mM) on the colorimetric reaction process.

2.6. Procedures for cholesterol detection

Cholesterol detection was done as follows: (a) 5 μL of CHOx (0.5 mg/mL) and 50 μL of various concentrations of cholesterol in 45 μL HAc-NAc (0.2 mM, pH 7.0) were incubated at 37 °C for 30 min; (b) 20 μL of MXene/CuS nanocomposites (2 mg/mL) and (c) 150 μL of HAc-NAc (0.2 mM, pH 3.5) and 40 μL of TMB (5 mM) were added into the above solution and then incubated at 37 °C for 10 min. UV–vis spectra measurements were taken and the product color was monitored at 652 nm. The final concentrations of cholesterol in the system varied from 0.1 mM to 1.0 mM. To identify the selectivity of our method, a variety of adding materials such as ascorbic acid, uric acid, glucose, cysteine and serine were investigated.

2.7. Total cholesterol detection in human serum samples

Human serum samples from three volunteers were collected from the first affiliated hospital of Zhengzhou University. Firstly, the serum samples were diluted 10 times using 0.5 mM Britton-Robinson (B-R) buffer solution (pH 7.4). Then, a 10 μL of the diluted serum was incubated with 50 μL cholesterol esterase (0.05 U/mL) for 5 min at 37 °C. Finally, a 40 μL B-R buffer solution was added into the solution. The subsequent procedure was the same with that of cholesterol detection above mentioned.

3. Results and discussion

3.1. Characterization of MXene-Ti_3C_2 and MXene/CuS nanocomposites

The exfoliation of Ti_3AlC_2 precursor was carried out using HCl–LiF etchant at room temperature. The SEM image of MXene-Ti_3C_2 (Fig. S1a) clearly showed that the layered structures were separated from each other, revealing accordion-like open morphology. A high magnification image (Fig. S1b) further showed that there were lots of submicro-scale and nanoscale spaces between the flakes, which provide substantive channels and active sites for Cu^{2+} ions intercalation. Under hydrothermal effect, CuS nanoparticles were formed between the flakes. As shown in Fig. 1a, the novel morphology characters of nanocomposites with some nanoparticles coated on each flake were observed, revealing a close combination hierarchical architecture of Mxene-Ti_3C_2 and CuS. It can be deduced that MXene-Ti_3C_2 served as templates for the growth of nanoparticle CuS on their surface. In addition, the distribution of CuS nanoparticles was uniform (Fig. S2). The EDX analysis in Fig. 1b demonstrated that the chemical components of nanocomposites consisted of Cu, S, C and Ti elements, further indicating the CuS nanoparticles are successfully combined with the MXene. XRD experiment was used to test the phase purity and crystallinity of the as-prepared MXene-Ti_3C_2/CuS nanocomposites. Compared with pristine MXene-Ti_3C_2 (Fig. 1c), several extra diffraction peaks located at 27.6°, 29.3°, 31.5°, 32.7°, 38.8°, 48.4°, 52.5°, and 59.1° were observed and indexed to the (100), (101), (102), (103), (105), (107), (108) and (203) planes of hexagonal phase CuS, which is in good agreement with the values reported (JCPDS 06-0464). Raman spectroscopy plays a key role in the structural characterization of MXene-Ti_3C_2/CuS nanocomposites. As shown in Fig. 1d, a strong and sharp band located at 474 cm^{-1} probably originates from the lattice vibration of CuS nanoparticles, which is very similar to the result reported by others.

More characterization of Mxene-Ti_3C_2 nanosheets and MXene-Ti_3C_2/CuS nanocomposites regarding the surface chemical environment and composition was carried out using XPS experiments. The XPS spectra of full survey in MXene-Ti_3C_2/CuS nanocomposite clearly present the signals intensity of Ti, C, Cu and S elements. However, only the signals of Ti and C elements appeared in widescreen XPS spectrum of MXene, which means that the efficient combination of MXene and CuS is finished, as shown in Fig. 2a. In order to further identify the binding nature of S and Cu elements, the peaks of S 2p and Cu 2p were studied by high resolution XPS spectra. As shown in Fig. 2b, there are two main peaks of S in the 2p region, located at 162.4 eV and 163.5 eV, assigning to S $2p_{3/2}$ and S $2p_{1/2}$. Since S^{2-} ions released from CuS and SO_4^{2-} from trace amount of $CuSO_4$, two more side peaks appeared at 163.2 eV and 168.4 eV. Also, Fig. 2c is a representing high resolution spectrum of Cu 2p. From it, one can clearly see that two strong peaks at 931.8 eV and 952.7 eV emerged, assigning to Cu $2p_{3/2}$ and Cu $2p_{1/2}$, respectively. The two peaks were separated by ca. 20.0 eV, indicating the presence of the identical binding energies for chemical states of Cu^{2+}. These results clearly demonstrated the existence of CuS on the Mxene-Ti_3C_2 nanosheets. FT-IR spectra were further used to analyze the surface structure of nanocomposites, as shown in Fig. 2d. There are two strong peaks located at 3420 cm^{-1} and 1625 cm^{-1}, which are attributed to the –OH or extremely coordinated H_2O in the samples of Mxene-Ti_3C_2 nanosheets and MXene-Ti_3C_2/CuS nanocomposites. The adsorption peaks at 596 cm^{-1} and 1120 cm^{-1} are on the account of Cu—S stretching modes and characteristic vibration [45]. It is worth noting that no absorption peaks were observed from 3800 to 500 cm^{-1}.

3.2. Peroxidase-like activity of MXene-Ti_3C_2/CuS nanocomposites and H_2O_2 detection

The as-synthesized MXene-Ti_3C_2/CuS nanocomposites were found

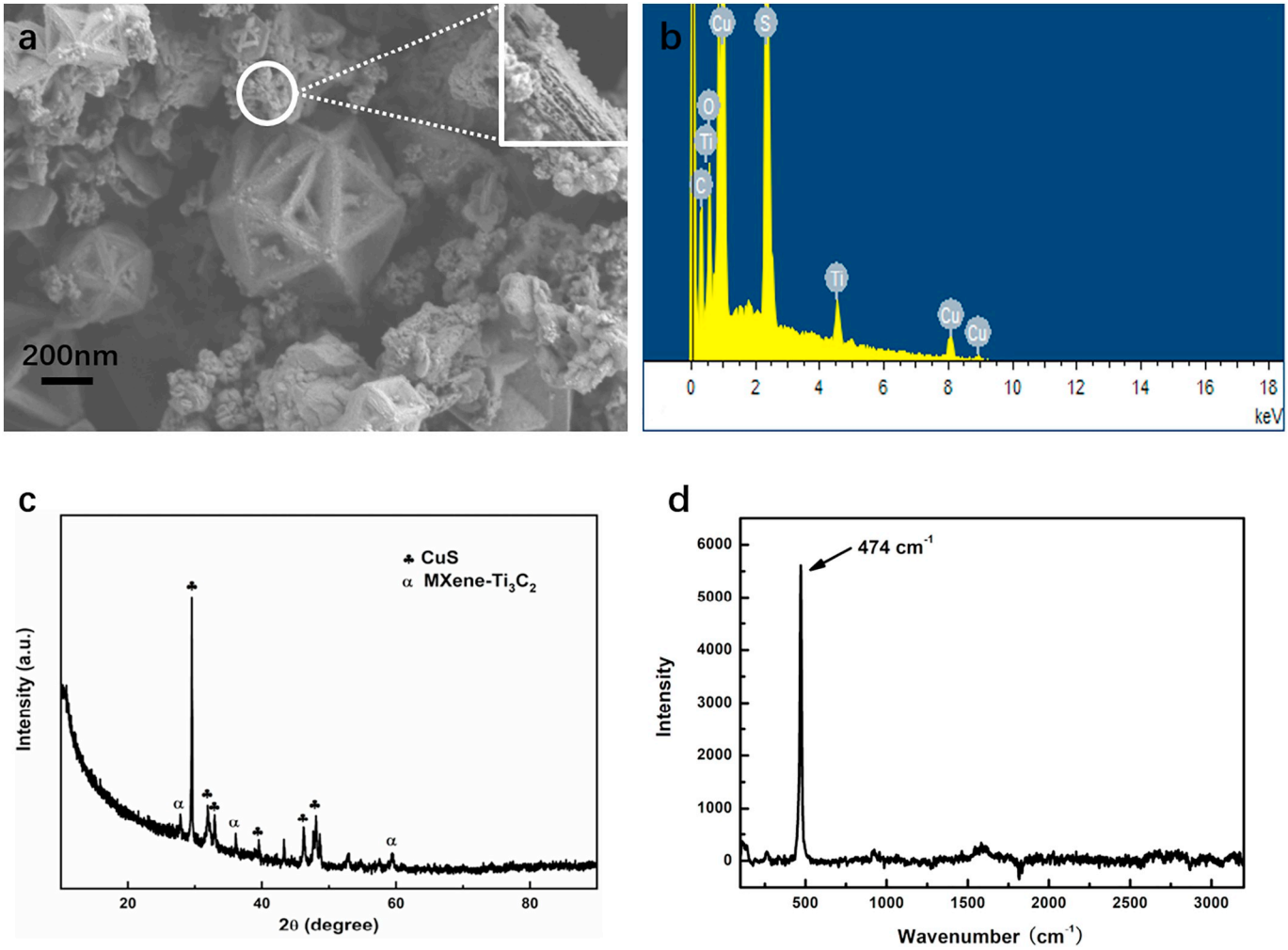

Fig. 1. (a) SEM, (b) EDX, (c) XRD and (d) Raman images of as-prepared MXene/CuS nanocomposites. Inset in (a): the partial enlarged detail of MXene-Ti_3C_2 nanosheets.

to exhibit a peroxidase-like activity. They could catalyze the oxidation substrate such as TMB, ABTS and OPD in the presence of H_2O_2 solution to promote a color change in HAc-NaAc buffer. The catalytic activity is dependent on both H_2O_2 concentration and MXene-Ti_3C_2/CuS nanocomposites concentration. Considering the less toxicity and good stability of TMB as substrate, MXene-Ti_3C_2/CuS-TMB-H_2O_2 system has been used to characterize the peroxidase-like activity in our experiment to produce a blue color product (TMB^{*+}). As shown in Fig. 3a, the absorbance peaks at 652 nm originated from the oxidation product of TMB gradually increased with time from 0 to 18 min, which is similar to the phenomenon observed using the enzyme-horseradish peroxidase (HRP). The linear relationship is shown in Fig. S3. These results demonstrated that the MXene-Ti_3C_2/CuS nanocomposites definitely have the typical catalysis behavior of peroxidase toward TMB substrate. In comparison to the other reaction systems, as shown in Fig. 3b, the CuS-TMB-H_2O_2 system also exhibited a peroxidase-like activity, but the catalytic efficiency is much lower than the MXene-Ti_3C_2/CuS-TMB-H_2O_2 system. Meanwhile, we find that the MXene-TMB-H_2O_2 has no any peroxidase-like activity. All of these show that the MXene-Ti_3C_2/CuS nanocomposite has a rapid initial reaction rate and an improved intrinsic peroxidase-like activity. Therefore, the MXene-Ti_3C_2/CuS-TMB-H_2O_2 is considered as the optimum research system in the following work. Furthermore, we surveyed the effects of pH and temperature to the activity of MXene-Ti_3C_2/CuS mimetic. The pH values changed from 3.0 to 5.0 and the temperature values changed from 30 °C to 55 °C are shown in Fig. 4. One can find that the MXene-Ti_3C_2/CuS nanocomposites exhibit a good activity at established pH and temperature, which is similar to other peroxidase-like nanomaterials reported in literatures. Maximum catalysis reaction activity was achieved at the pH 3.5 and temperature at 55 °C. To be noticed, the temperature has little influence to the catalysis activity, indicating that the MXene-Ti_3C_2/CuS nanocomposite possesses strong temperature resistance ability. This is beneficial to the wide-range application of this material. Thus, MXene-Ti_3C_2/CuS-TMB-H_2O_2 could be regarded as a temperature-friendly reaction system in the application of biosensor and detection assay.

In order to address the next important parameter of the steady-state kinetics, the catalytic mechanism of the peroxidase-like activity of MXene-Ti_3C_2/CuS was investigated by changing the reaction concentrations of TMB and H_2O_2. As shown in Fig. 5, the typical Michaelies-Menten curves were obtained under the optimum pH and the room temperature for TMB and H_2O_2, respectively. The K_m and V_{max} were calculated from Lineweaver-Burk plots. The equation $1/V_0 = (K_m/V_{max})\cdot(1/[S]) + 1/V_{max}$, where K_m is an indicator of the affinity of enzyme for one substrate. The smaller the value of K_m, the stronger is the affinity between the enzyme and the substrate. We listed the values of K_m and V_{max} in this study (Table 1.) and compared them with other peroxidase-like activity nanomaterials. For the K_m value of MXene-Ti_3C_2/CuS nanocomposites catalyzed the substrate TMB was 0.072 mM, which is lower than BNNSs@CuS nanohybrid, CuS cluster and GO-Fe_3O_4 nanocomposite [45,47]. This indicated that the MXene-Ti_3C_2/CuS nanocomposites have a higher affinity for TMB than some reported

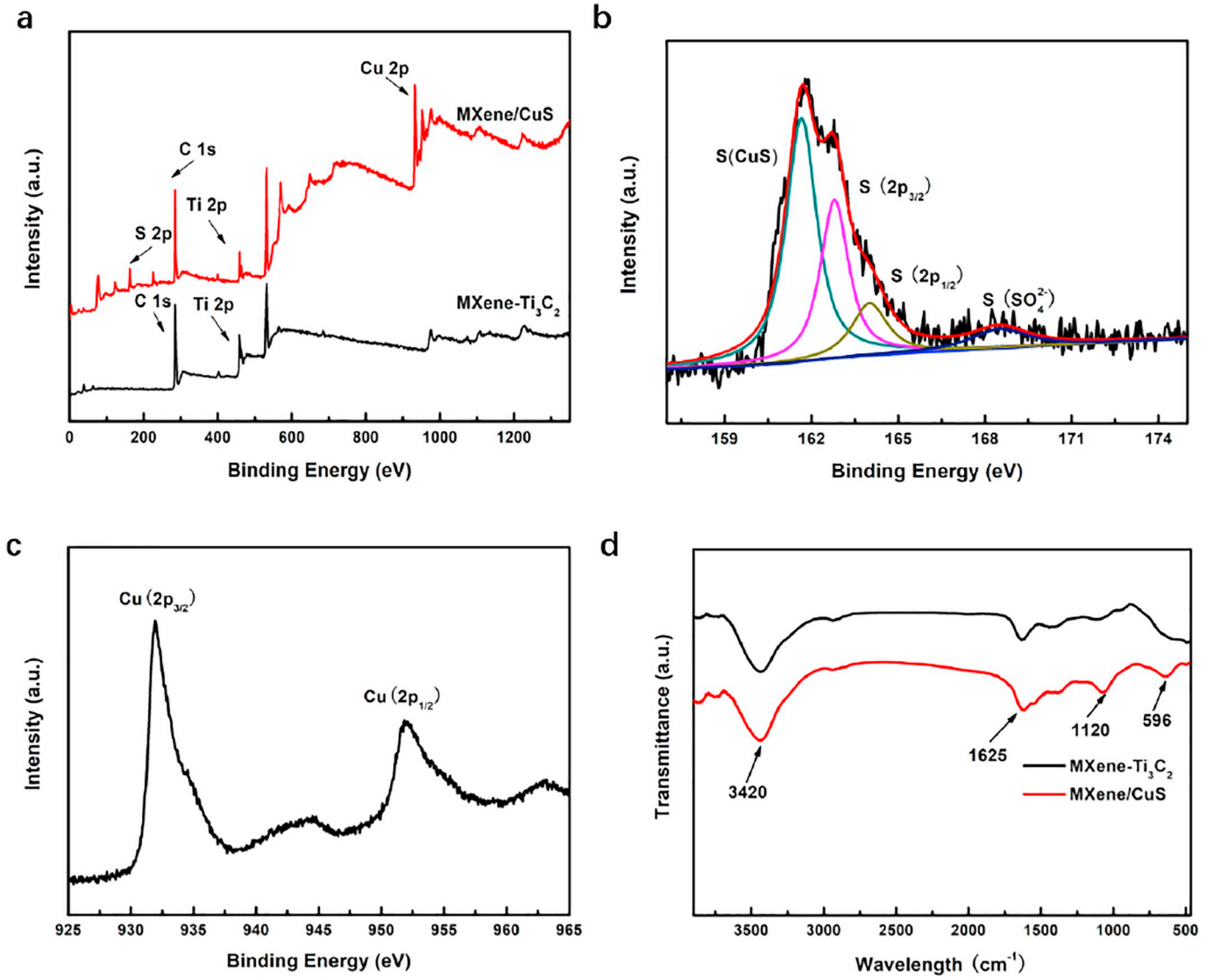

Fig. 2. (a) XPS spectra of full survey spectrum, (b) XPS spectra of S 2p, (c) XPS spectra of Cu 2p and (d) FT-IR spectra of MXene-Ti_3C_2 nanosheets and MXene-Ti_3C_2/CuS nanocomposites.

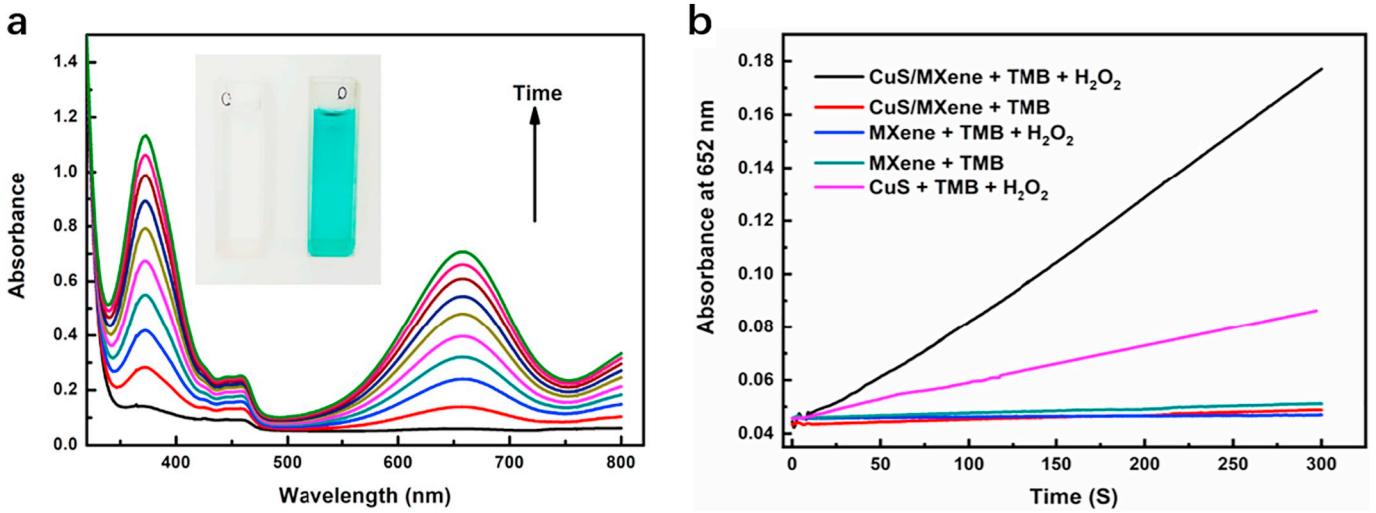

Fig. 3. (a) Time-dependent UV–vis spectral changes of MXene-Ti_3C_2/CuS-TMB-H_2O_2 system; (b) time-dependent absorbance changes of TMB at 652 nm for different reaction systems in HAc-NaAc buffer (pH 3.5) at room temperature.

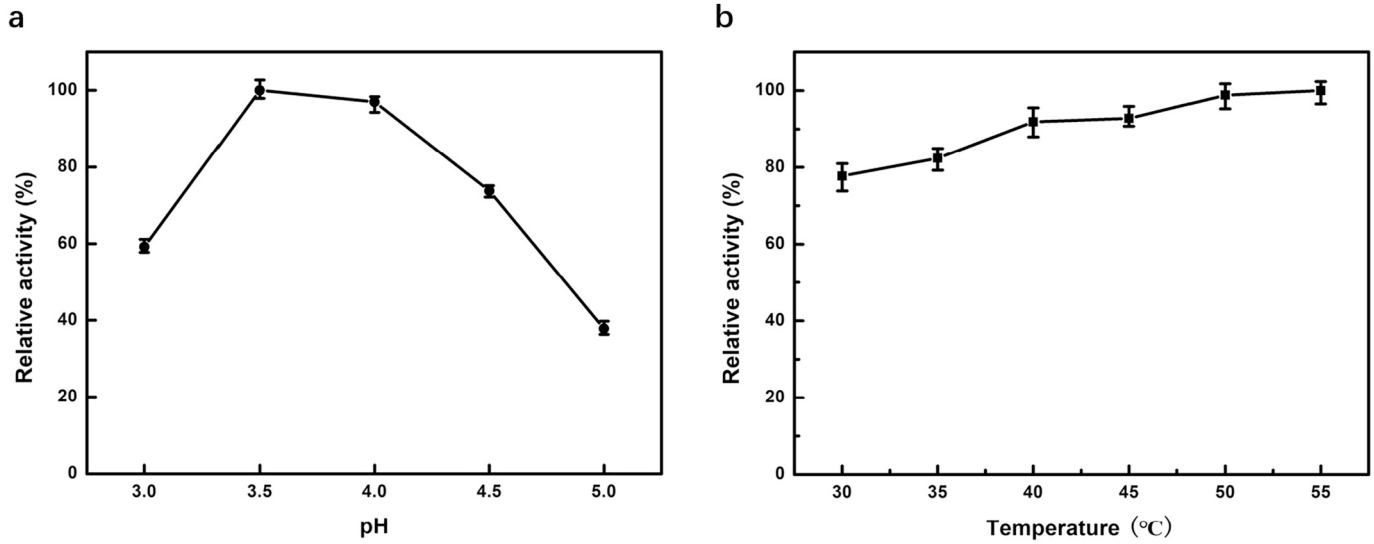

Fig. 4. (a) The effects of different pH values for peroxidase-like MXene-Ti_3C_2/CuS catalysis activities of TMB; (b) the effects of various temperature for peroxidase-like MXene-Ti_3C_2/CuS catalysis activities of TMB.

nanomaterials. It may be derived from some characters of this nanocomposite such as its large surface area, strong adsorption ability, the accelerated charge transfer from TMB to H_2O_2 by increasing the electronic density and mobility in the MXene-Ti_3C_2 matrix, as well as a high conductivity of MXene-Ti_3C_2 nanosheets. However, the K_m value of MXene/CuS nanocomposites with H_2O_2 as the substrate is 2.08, which is apparently much higher than that of BSA-MnO_2 and GO-Fe_3O_4 [47,48]. It is consistent with the fact that a lower H_2O_2 concentration was required to get the maximal level of peroxidase-like activity of MXene-Ti_3C_2/CuS nanocomposite. In addition, we tested its activity over a range of H_2O_2 and TMB. As shown in Fig. S4, the slopes of all lines are almost parallel, which is an obvious character of a ping-pong mechanism for this colorimetric reaction. This result also inspire us to deduce the mechanism may be as following: at first, MXene-Ti_3C_2/CuS nanocomposites react with H_2O_2 to form an intermediate peroxide species, and then, the reactive species further reach with the TMB substrate by the nucleophilic attack, leading to TMB be oxidized to form the TMB^{*+} species, finally, the color changes from colorless to blue. Here, the function of the MXene-Ti_3C_2/CuS nanocomposites is to accelerate the electron-transfer process and stimulate the generation of free radicals.

Table 1
Comparison of the Michaelis-Menten constants (K_m) and maximum reaction rates (V_{max}) among several nanomaterials and enzymes.

Catalyst	K_m (mM)		V_{max} (10^{-8} M·S^{-1})		Reference
	TMB	H_2O_2	TMB	H_2O_2	
CuS cluster	0.648	29.16	5.96	4.22	[50]
BNNS@CuS	0.175	25	3.76	12.5	[51]
PB-Fe_2O_3	0.00995	15	0.123	0.228	[52]
GO-Fe_3O_4	0.43	0.71	13.08	5.31	[53]
BSA-MnO_2	0.04	0.12	578	5.71	[54]
GQD	0.01	8	0.073	0.117	[55]
HRP	0.434	3.70	10.0	8.71	[56]
MXene/CuS	0.072	2.08	4.63	6.34	Present work

To utilize the intrinsic peroxidase-like property of MXene-Ti_3C_2/CuS nanocomposites, a simple colorimetric method to detect H_2O_2 was

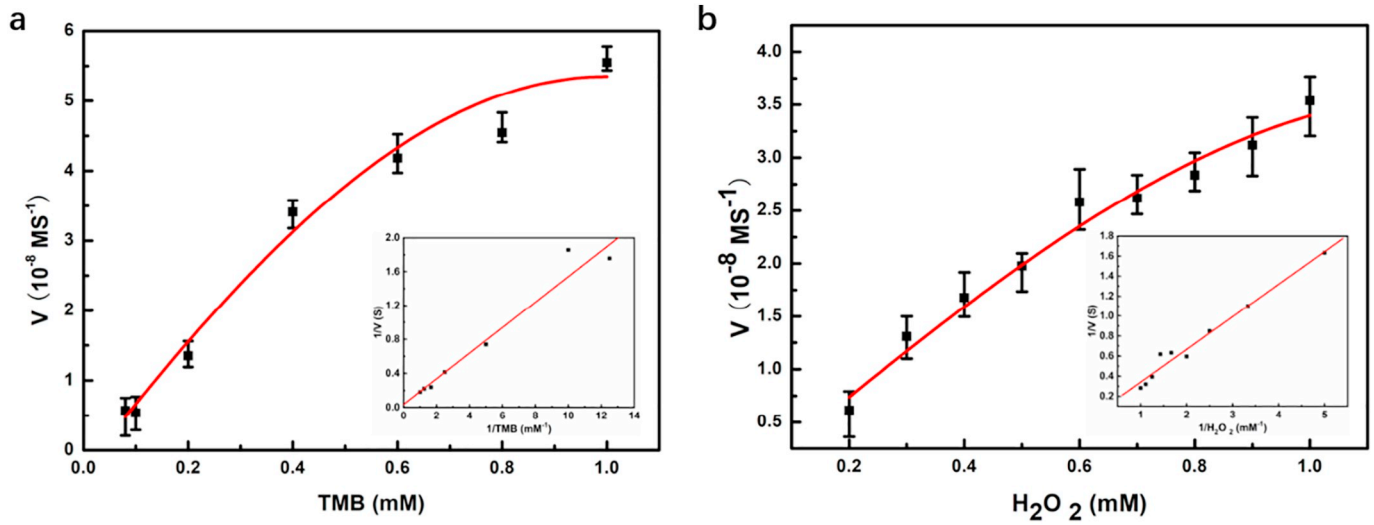

Fig. 5. Steady-state kinetic assay of MXene-Ti_3C_2/CuS nanocomposites, the reaction was measured using 2.0 mg/ mL MXene/CuS nanocomposites in pH 3.5 HAc-NaAc buffer at room temperature. (a) The concentration of H_2O_2 is 100 mM. (b) The concentration of TMB was 1.0 mM. Insets are the Lineweaver-Burk plots of the double reciprocal of the Michaelis-Menten equation.

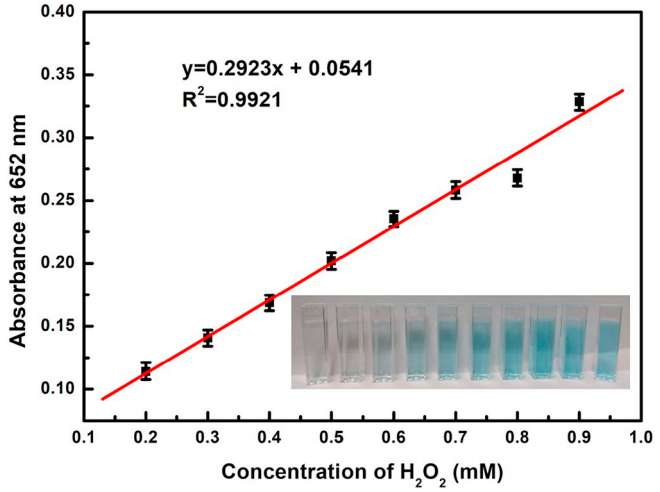

Fig. 6. The linear standard curve for H_2O_2 determination. Inset: the color change corresponding to different concentrations of H_2O_2.

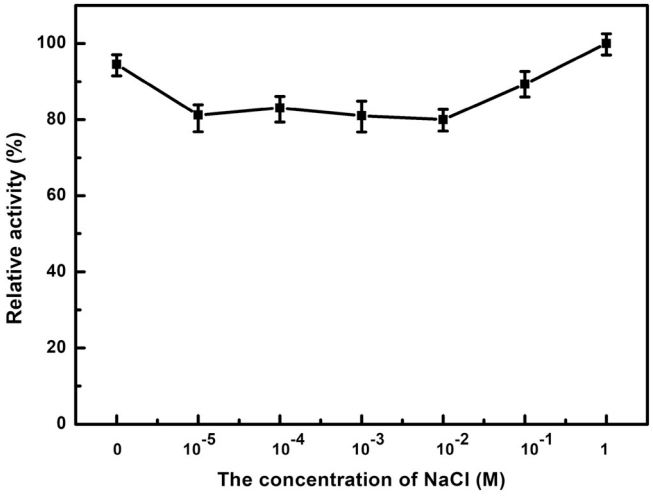

Fig. 7. Influence of different concentrations of NaCl solution for MXene-Ti_3C_2/CuS catalytic activity in the presence of TMB and H_2O_2.

Table 2
Comparison of the performances of various sensing materials for H_2O_2 detection.

Sensing materials	Detection mode	LOD (μM)	Linear range (μM)	Reference
CuS cluster	Colorimetry	10	10–1000	[50]
BNNSs@CuS	Colorimetry	4.7	100–1000	[51]
MoS_2	Colorimetry	1.5	5–100	[57]
GO-Fe_3O_4	Colorimetry	0.32	1–50	[53]
MnSe	Colorimetry	0.085	0.17–10	[58]
Au particle	Colorimetry	5	2–200	[59]
GQD	Colorimetry	9	10–100	[55]
MXene/CuS	Colorimetry	3.1	100–1000	Present work

developed in next work. The absorbance of oxidized TMB product concentration is in proportion to that of H_2O_2. Therefore, it is a facile approach to detect H_2O_2 at 652 nm UV–vis absorption. From Fig. 6, one can find that a line increase in the absorbance intensity was obtained as the concentration of H_2O_2 ranging from 0.1 mM to 1.0 mM. The color change during the reaction can be obviously visual (Fig. 6, inset), which provides us a convenient and fast approach to detect H_2O_2 by naked eye. The calibration curve was plotted by the linear fitting. LOD was calculated by the formula of LOD = 3σ/slope, where σ was the standard deviation of blank. A detection limit of H_2O_2 is calculated as 3.1 μm, which is lower than that of reported CuS cluster, BNNSs@CuS nanohybrid and MoS_2 nanosheets [45,49], as listed in Table 2.

Since the ionic strength has an important influence in the colorimetric reaction system, we also study NaCl concentrations to affect the relatively activity of MXene-Ti_3C_2/CuS mimetics. NaCl performs as an indispensable and crucial electrolyte in human body, which is regarded as the influencing factor in this reaction environment. As shown in Fig. 7, the NaCl concentrations ranging from 0 to 1 M has little influence on the catalytic activity of MXene-Ti_3C_2/CuS nanocomposites. It is worth noting that the concentration of NaCl in human blood is 0.154 M within the range of our detection, revealing that the MXene-Ti_3C_2/CuS nanocomposites can be used for practical sample detection in human blood.

In medicine, cholesterol is a very important biochemical indicator, and its concentration in human blood is of great significance for preventing the risk of cardiovascular diseases. Therefore, people should pay much attention to the content and treatment of cholesterol. On the other hand, hydrogen peroxide is the main product of cholesterol oxidase-catalyzed cholesterol reaction. Therefore, colorimetric detection of cholesterol can also be completed using MXene-Ti_3C_2/CuS nanocomposites instead of traditionally used peroxidase. The MXene-Ti_3C_2/CuS nanocomposites are used for the colorimetric determination of cholesterol with a linear range of 10–100 μm and a limit of detection (LOD) is 1.9 μm, as shown in Fig. 8. The calculation formula of LOD is consistent with the detection limit of hydrogen peroxide mentioned above.

3.3. Comparison of sensing performances

The analytical performance of MXene-Ti_3C_2/CuS based cholesterol biosensor is further compared with other nanomaterials-based assays in terms of detection mode, LOD, as well as linear range. As shown in Table 3, we listed two popular detection modes (amperometric, electrochemiluminescence and colorimetry) for cholesterol determination. In comparison with similar colorimetric detection based on boron nitride nanosheet and copper sulfide nanohybrids (BNNS@CuS) and graphene quantum dots (GQD), the MXene-Ti_3C_2/CuS nanocomposites exhibit 1–4 times improvement on detection limits and the linear range is also similar or lower, especially GQD. This indicates that our used material has excellent performance among similar materials. However, compared with some reported electrochemical method, the MXene-Ti_3C_2/CuS nanocomposite based colorimetric sensing is more sensitive than some electrochemical nanomaterials, and is less sensitive than others. Although not as sensitive as some electrochemical-sensing nanomaterials, our method avoids the tedious preparation and modification of electrodes. Importantly, the proposed MXene-Ti_3C_2/CuS-based colorimetric approach displayed a high selectivity for cholesterol detection. Some possible interfering species (such as ascorbic acid, glucose, uric acid, cysteine and serine) existed in blood were studied. As shown in Fig. 9, our results indicated that these interfering species had little influence on UV-absorbance of cholesterol or even a higher concentration (up to 4 times cholesterol concentration) is used.

3.4. Determination of total cholesterol in real samples

It is universally recognized that the level of cholesterol in blood should be strictly controlled due to its risks to cardiovascular diseases. Herein, to verify the actual application potentials of MXene-Ti_3C_2/CuS nanocomposite based biosensor, the real cholesterol detection in human blood is carried out under optimum condition. It is noted that serum includes cholesterol esters and free cholesterol. To measure the total cholesterol level, Cholesterol esterase is added, which can effectively turn cholesterol esters into cholesterol. Furthermore, the three analyses are repeated for 3 times by a standard addition under the same

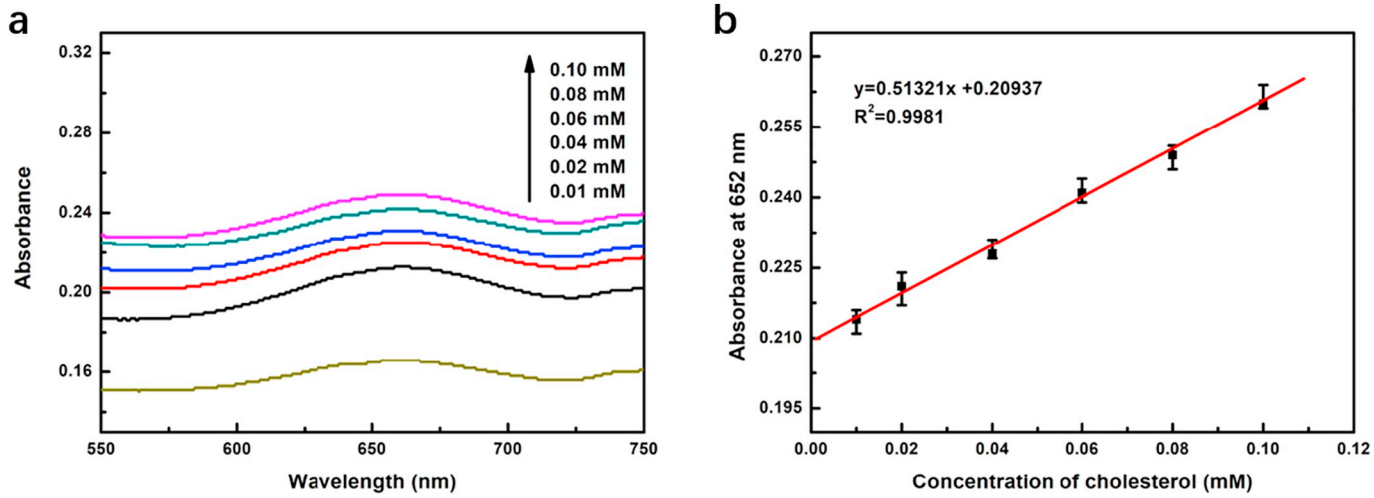

Fig. 8. (a) UV–vis spectra of the mixed solutions of TMB and MXene-Ti_3C_2/CuS in pH 3.5 HAc-NaAc buffer at 37 °C. The TMB concentration was 5 mM, and 5 μL CHOx and 20 μL MXene-Ti_3C_2/CuS dispersions were used. (b) The linear standard curve for cholesterol determination.

condition. Table 4 shows the results of cholesterol in human serum. The values measured by our method are highly consistent with the ones obtained from the First Affiliated Hospital of Zheng Zhou University and a relative standard deviation of 3.1% (n = 7) was obtained. When 4 mM cholesterol is added to the serum samples, the recovery values obtained are 94.1, 94.3%, and 93.7%, respectively. These results show that the as-prepared biosensor can be implemented for the detection of total cholesterol in clinic. In addition, since the obvious color change (from colorlessness to blue) can be easily recognized by naked eye, it is convenient for analysts to qualitatively judge the primary results without complex instruments or procedures.

4. Conclusion

In summary, MXene-Ti_3C_2/CuS nanocomposites possessing intrinsic peroxidase-like activity were successfully prepared through a simple hydrothermal approach. The catalysis performance is closely associated with pH, temperature and H_2O_2 concentration. In comparison with individual MXene and CuS nanomaterials, MXene-Ti_3C_2/CuS nanocomposite as a novel mimic peroxidase showed enhanced catalytic activity and the catalysis follows a ping-pong mechanism. In the presence of cholesterol oxidase and TMB, the MXene/CuS nanocomposites based colorimetric sensor showed an outstanding performance for cholesterol determination with a broad linear range of 10–100 μM and a limit of detection (LOD) of 1.9 μM, which is more sensitive than many reported other methods. In addition, the selectivity is also satisfied. Our work indicated that MXene-Ti_3C_2/CuS nanocomposites can be used as promising candidates for colorimetric detection of cholesterol, glucose, dopamine etc.

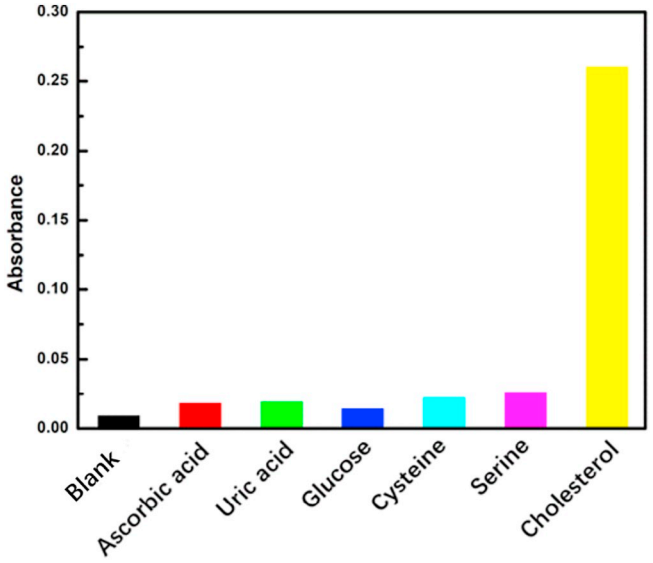

Fig. 9. Selectivity analysis for cholesterol detection by monitoring the absorbance.

Acknowledgments

This work was supported by the National Natural Science Foundation of China (81472001, 31400851), the Minjiang Scholars Program of Fujian Province, the Tongjiang Scholars Program of Quanzhou City, Quanzhou City Science & Technology Program of China, and the Fourth Health Education Joint Development Project of Fujian Province (WKJ-2016-2-36).

Table 3
Performances of various modified cholesterol sensing methods and materials.

Sensing materials	Detection mode	LOD (μM)	Linear range (μM)	Reference
ChOx/PEDOT/PMB/GCE	Amperometric	1.6	0.01–0.22	[60]
MWCNTs–ChOxSiO$_2$-chitosan/PB/GCE	Amperometric	1	4–700	[61]
ChOx/CoOx NPs/GCE	Amperometric	4.2	4.2–50	[62]
ChOx/hemoglobin	Amperometric	9.5	10–600	[63]
AgNPs-BSA-MnO_2	Electrochemiluminescence	0.07	0.21–1667	[64]
GQD	Colorimetry	6	20–600	[55]
BNNSs@CuS	Colorimetry	2.9	10–100	[51]
MXene/CuS	Colorimetry	1.9	10–100	Present work

Table 4
Determination of total cholesterol in human serum samples.

Sample	C[a]	C[b]	Added	Found	Recovery
	($mmol \cdot L^{-1}$)		($mmol \cdot L^{-1}$)		(%)
S1	4.02	3.96 ± 0.13	4.00	7.76 ± 0.05	95.1
S2	4.32	4.21 ± 0.13	4.00	8.03 ± 0.05	95.5
S3	4.50	4.40 ± 0.12	4.00	8.05 ± 0.05	91.3

[a] Determined the human serum sample in the hospital.
[b] Determined the human serum sample by using the MXene/CuS nanocomposites.

Appendix A. Supplementary data

Supplementary data to this article can be found online at https://doi.org/10.1016/j.msec.2019.110000.

References

[1] N. Wang, J. Sun, L. Chen, H. Fan, S. Ai, Microchim. Acta 182 (2015) 1733–1738.
[2] W.J. Shi, H. Fan, S.Y. Ai, L.S. Zhu, Sensors Actuators B Chem. 221 (2015) 1515–1522.
[3] W. He, J. Cai, H. Zhang, L. Zhang, X. Zhang, J. Li, J.-J. Yin, ACS Appl. Nano Mater. 1 (2018) 222–231.
[4] C. Hu, D.-P. Yang, F. Zhu, F. Jiang, S. Shen, J. Zhang, ACS Appl. Mater. Interfaces 6 (2014) 4170–4178.
[5] N.R. Nirala, S. Pandey, A. Bansal, V.K. Singh, B. Mukherjee, P.S. Saxena, A. Srivastava, Biosens. Bioelectron. 74 (2015) 207–213.
[6] Y. Huang, J. Tan, L. Cui, Z. Zhou, S. Zhou, Z. Zhang, R. Zheng, Y. Xue, M. Zhang, S. Li, N. Zhu, J. Liang, G. Li, L. Zhong, Y. Zhao, Biosens. Bioelectron. 102 (2018) 560–567.
[7] J. Li, T. Liu, S. Liu, J. Li, G. Huang, H.H. Yang, Biosens. Bioelectron. 120 (2018) 137–143.
[8] T. Lin, L. Zhong, H. Chen, Z. Li, Z. Song, L. Guo, F. Fu, Microchim. Acta 184 (2017) 1233–1237.
[9] B.K. Shrestha, R. Ahmad, S. Shrestha, C.H. Park, C.S. Kim, Biosens. Bioelectron. 94 (2017) 686–693.
[10] Y. Huang, L. Cui, Y. Xue, S. Zhang, N. Zhu, J. Liang, G. Li, Mater. Sci. Eng. C Mater. Biol. Appl. 77 (2017) 1–8.
[11] Y. He, X. Niu, L. Shi, H. Zhao, X. Li, W. Zhang, J. Pan, X. Zhang, Y. Yan, M. Lan, Microchim. Acta 184 (2017) 2181–2189.
[12] X. Li, Z. Pu, H. Zhou, W. Zhang, X. Niu, Y. He, X. Xu, F. Qiu, J. Pan, L. Ni, J. Mater. Sci. 53 (2018) 13912–13923.
[13] F. Xie, X. Cao, F. Qu, A.M. Asiri, X. Sun, Sensors Actuators B Chem. 255 (2018) 1254–1261.
[14] J. Lv, C. Kong, K. Liu, L. Yin, B. Ma, X. Zhang, S. Yang, Z. Yang, Chem. Commun. 54 (2018) 8458–8461.
[15] Q. Liu, T. Zhang, L. Yu, N. Jia, D.-P. Yang, Analyst 138 (2013) 5559.
[16] J. Cui, S. Jia, Coord. Chem. Rev. 352 (2017) 249–263.
[17] H. Wei, E. Wang, Chem. Soc. Rev. 42 (2013) 6060–6093.
[18] Z.S. Al-Garawi, B.A. McIntosh, D. Neill-Hall, A.A. Hatimy, S.M. Sweet, M.C. Bagley, L.C. Serpell, Nanoscale 9 (2017) 10773–10783.
[19] Y. Liu, M. Yuan, L. Qiao, R. Guo, Biosens. Bioelectron. 52 (2014) 391–396.
[20] J. Chen, J. Wang, Y. Bai, K. Li, E.S. Garcia, A.L. Ferguson, S.C. Zimmerman, J. Am. Chem. Soc. 140 (2018) 13695–13702.
[21] Y. Tao, E. Ju, J. Ren, X. Qu, Adv. Mater. 27 (2015) 1097–1104.
[22] D.H. Kim, J. Hur, H.G. Park, M. Il Kim, Biosens. Bioelectron. 93 (2017) 226–233.
[23] S.C. Min Su Kim, H.J. Se, J. Lee, S.K. Kwak, M.I. Kim, J. Lee, ACS Nano 13 (2019) 4312–4321.
[24] M.I. Kim, J. Shim, T. Li, J. Lee, H.G. Park, Chemistry 17 (2011) 10700–10707.
[25] B. Liu, J. Liu, Nano Res. 10 (2017) 1125–1148.
[26] Y. Fan, W. Shi, X. Zhang, Y. Huang, J. Mater. Chem. A 2 (2014) 2482.
[27] Z. Tian, J. Li, Z. Zhang, W. Gao, X. Zhou, Y. Qu, Biomaterials 59 (2015) 116–124.
[28] H.J. Cheon, M.D. Adhikari, M. Chung, T.D. Tran, J. Kim, M.I. Kim, Adv. Healthc. Mater. 8 (2019) 1801507.
[29] L. Han, C. Li, T. Zhang, Q. Lang, A. Liu, ACS Appl. Mater. Interfaces 7 (2015) 14463–14470.
[30] C. Ge, R. Wu, Y. Chong, G. Fang, X. Jiang, Y. Pan, C. Chen, J.-J. Yin, Adv. Funct. Mater. 28 (2018) 1801484.
[31] Z. Yang, J. Qian, X. Yang, D. Jiang, X. Du, K. Wang, H. Mao, K. Wang, Biosens. Bioelectron. 65 (2015) 39–46.
[32] A. Sun, L. Mu, X. Hu, ACS Appl. Mater. Interfaces 9 (2017) 12241–12252.
[33] M.I. Kim, Y. Ye, B.Y. Won, S. Shin, J. Lee, H.G. Park, Adv. Funct. Mater. 21 (2011) 2868–2875.
[34] H. Zhao, Y. Dong, P. Jiang, G. Wang, J. Zhang, ACS Appl. Mater. Interfaces 7 (2015) 6451–6461.
[35] X. Niu, X. Xu, X. Li, J. Pan, F. Qiu, H. Zhao, M. Lan, Chem. Commun. 54 (2018) 13443–13446.
[36] J. Mu, J. Li, X. Zhao, E.-C. Yang, X.-J. Zhao, Sensors Actuators B Chem. 258 (2018) 32–41.
[37] Z. Yang, Y. Zhu, M. Chi, C. Wang, Y. Wei, X. Lu, J. Colloid Interface Sci. 511 (2018) 383–391.
[38] J. Liu, L. Meng, Z. Fei, P.J. Dyson, X. Jing, X. Liu, Biosens. Bioelectron. 90 (2017) 69–74.
[39] L. He, Y. Lu, F. Wang, W. Jing, Y. Chen, Y. Liu, Sensors Actuators B Chem. 254 (2018) 468–474.
[40] K. Huang, Z. Li, J. Lin, G. Han, P. Huang, Chem. Soc. Rev. 47 (2018) 5109–5124.
[41] J. Zhu, E. Ha, G. Zhao, Y. Zhou, D. Huang, G. Yue, L. Hu, N. Sun, Y. Wang, L.Y.S. Lee, C. Xu, K.-Y. Wong, D. Astruc, P. Zhao, Coord. Chem. Rev. 352 (2017) 306–327.
[42] B. Xu, M. Zhu, W. Zhang, X. Zhen, Z. Pei, Q. Xue, C. Zhi, P. Shi, Adv. Mater. 28 (2016) 3333–3339.
[43] M. Soleymaniha, M.-A. Shahbazi, A.R. Rafieerad, A. Maleki, A. Amiri, Adv. Healthc. Mater. (2018) 1801137.
[44] J. Huang, J. Zhou, J. Zhuang, H. Gao, D. Huang, L. Wang, W. Wu, Q. Li, D.P. Yang, M.Y. Han, ACS Appl. Mater. Interfaces 9 (2017) 36606–36614.
[45] Y. Zhang, Y.-N. Wang, X.-T. Sun, L. Chen, Z.-R. Xu, Sensors Actuators B Chem. 246 (2017) 118–126.
[46] G. Liu, J. Zou, Q. Tang, X. Yang, Y. Zhang, Q. Zhang, W. Huang, P. Chen, J. Shao, X. Dong, ACS Appl. Mater. Interfaces 9 (2017) 40077–40086.
[47] Y.L. Dong, H.G. Zhang, Z.U. Rahman, L. Su, X.J. Chen, J. Hu, X.G. Chen, Nanoscale 4 (2012) 3969–3976.
[48] X. Liu, Q. Wang, H. Zhao, L. Zhang, Y. Su, Y. Lv, Analyst 137 (2012) 4552–4558.
[49] T. Lin, L. Zhong, L. Guo, F. Fu, G. Chen, Nanoscale 6 (2014) 11856–11862.
[50] G. Xu, L. Hu, et al., Copper nanoclusters as peroxidase mimetics and their applications to H_2O_2 and glucose detection, Anal. Chim. Acta 762 (1) (2013) 83–86.
[51] Y. Zhang, Y.N. Wang, X.T. Sun, et al., Boron nitride nanosheet/CuS nanocomposites as mimetic peroxidase for sensitive colorimetric detection of cholesterol, Sensors Actuators B Chem. 246 (2017) 118–126.
[52] A.K. Dutta, S.K. Maji, D.N. Srivastava, et al., Peroxidase-like activity and amperometric sensing of hydrogen peroxide by Fe_2O_3, and Prussian Blue-modified Fe_2O_3, nanoparticles, J. Mol. Catal. A Chem. 360 (8) (2012) 71–77.
[53] Y.L. Dong, H.G. Zhang, Z.U. Rahman, et al., Graphene oxide-Fe_3O_4 magnetic nanocomposites with peroxidase-like activity for colorimetric detection of glucose, Nanoscale 4 (13) (2012) 3969–3976.
[54] X. Liu, Q. Wang, H. Zhao, et al., BSA-templated MnO_2 nanoparticles as both peroxidase and oxidase mimics, Analyst 137 (19) (2012) 4552–4558.
[55] N.R. Nirala, S. Abraham, V. Kumar, et al., Colorimetric detection of cholesterol based on highly efficient peroxidase mimetic activity of graphene quantum dots, Sensors Actuators B Chem. 218 (2015) 42–50.
[56] L. Gao, J. Zhuang, L. Nie, et al., Intrinsic peroxidase-like activity of ferromagnetic nanoparticles, Nat. Nanotechnol. 2 (9) (2007) 577–583.
[57] T. Lin, L. Zhong, L. Guo, et al., Seeing diabetes: visual detection of glucose based on the intrinsic peroxidase-like activity of MoS_2 nanosheets, Nanoscale 6 (20) (2014) 11856–11862.
[58] F. Qiao, L. Chen, X. Li, et al., Peroxidase-like activity of manganese selenide nanoparticles and its analytical application for visual detection of hydrogen peroxide and glucose, Sensors Actuators B Chem. 193 (3) (2014) 255–262.
[59] Y. Jv, B. Li, R. Cao, Positively-charged gold nanoparticles as peroxidase mimic and their application in hydrogen peroxide and glucose detection, Chem. Commun. 46 (42) (2010) 8017–8019.
[60] S. Kakhki, M.M. Barsan, E. Shams, et al., New redox and conducting polymer modified electrodes for cholesterol biosensing, Anal. Methods 5 (5) (2013) 1199–1204.
[61] X. Tan, M. Li, P. Cai, et al., An amperometric cholesterol biosensor based on multiwalled carbon nanotubes and organically modified sol-gel/chitosan hybrid composite film, Anal. Biochem. 337 (1) (2005) 111–120.
[62] S. Aravamudhan, N.S. Ramgir, S. Bhansali, Electrochemical biosensor for targeted detection in blood using aligned Au nanowires, Sensors Actuators B Chem. 127 (1) (2007) 29–35.
[63] C. Zhao, L. Wan, L. Jiang, et al., Highly sensitive and selective cholesterol biosensor based on direct electron transfer of hemoglobin, Anal. Biochem. 383 (1) (2008) 25–30.
[64] D.P. Yang, W. Guo, Z. Cai, et al., Highly sensitive electrochemiluminescence biosensor for cholesterol detection based on AgNPs-BSA-MnO_2, nanosheets with superior biocompatibility and synergistic catalytic activity, Sensors Actuators B Chem. 260 (2018) 642–649.